ORIGINAL PAPER

Modelling and numerical simulation of the human aortic arch under in vivo conditions

Claudio M. García-Herrera · Diego J. Celentano

Abstract This work presents the modelling and simulation of the mechanical behaviour of the human aortic arch under in vivo conditions with pressure levels within the normal and hypertension physiological range. The cases studied correspond to young and aged arteries without cardiovascular pathologies. First, the tissue of these two groups is characterised via in vitro tensile test measurements that make it possible to derive the material parameters of a hyperelastic isotropic constitutive model. Then, these material parameters are used in the simulation of young and aged aortic arches subjected to in vivo normal and hypertension conditions. Overall, the numerical results were found not only to provide a realistic description of the mechanical behaviour of the vessel but also to be useful data that allow the adequate definition of stress/stretch-based criteria to predict its failure.

Keywords Human aortic arch · In vivo conditions · Finite elements · Modelling and simulation

1 Introduction

The human aortic arch is an elastic artery whose mechanical properties play a crucial role in damping the pressure wave that occurs inside the vessel and, in addition, to influence the blood flow coming from the heart (Nichols and Rourke 1990).

C. M. García-Herrera (✉)
Departamento de Ingeniería Mecánica, Universidad de
Santiago de Chile, USACH, Av. Bernardo O'Higgins 3363,
Santiago de Chile, Chile
e-mail: claudio.garcia@usach.cl

D. J. Celentano
Departamento de Ingeniería Mecánica y Metalúrgica, Pontificia
Universidad Católica de Chile, Av. Vicuña Mackenna 4860,
Santiago de Chile, Chile

Moreover, knowledge about the rupture stress and strain in this artery under normal, hypertension and severe (e.g. automobile accidents or cardiovascular problems) physiological conditions is also a relevant area of current interest (Richens et al. 2002; Field and Richens 2006; De Caro et al. 2007). The aortic arch motion is linked to that of the heart left ventricle through the aortic root. This motion generates axial stresses in the ascending aorta. Beller et al. (2005) consider that the motion of the aortic root induces high stress levels in the aortic arch that, in turn, may cause an aortic dissection even in patients without other risk factors. The surgical operation aimed at preventing the rupture of the aortic arch remains a risky procedure (Ergin et al. 1999) that is recommended only when the risk of failure of the artery wall is greater than that associated with the operation itself. Such a decision is based mainly on the dimensions of the vessel without taking into account its mechanical strength. Although the maximum artery diameter of 50 mm is usually taken as the criterion calling for surgery, 23% of the arteries fail before reaching this threshold (Erbel and Eggebrecht 2006; Pape et al. 2007). All these facts clearly justify the need for achieving a better understanding of the mechanical response of the human aortic arch. This is usually tackled via numerical simulations that predict the mechanical response of the artery in order to quantify its risk of failure under different loading conditions. In this context, one of the major challenges is the definition of realistic and reliable stress–strain relationships of the vessel (Demiray 1972; Delfino et al. 1997; Holzapfel et al. 2007; Doyle et al. 2010, 2012).

Numerical simulations have been performed recently to predict the mechanical response of the human aortic arch. Beller et al. (2004) and Beller et al. (2005) studied aortic arches under physiological conditions (in patients with and without aortic insufficiency) by means of a linear elastic isotropic constitutive model and boundary conditions that

accounted for experimentally measured aortic root displacements during the cardiac cycle. However, the effect of the ligamentum arteriosum was not included in the analysis. Both aortic root displacement and hypertension were found to significantly increase the longitudinal stress in the ascending aorta. Gao et al. (2006) performed a study of the stress distribution in a layered aortic arch model (also using a linear elastic isotropic law) with interaction between a pulsatile flow and the wall of the blood vessel. This work indicates that the circumferential stress in the aortic wall is directly associated with the blood pressure, supporting the clinical importance of blood pressure control. Moreover, another relevant aspect that should be addressed in numerical simulations under in vivo conditions is the definition of a representative initial configuration of the aortic arch. This can be firstly achieved by means of clinical techniques, e.g. computed tomography (CT) and angiography, that afterwards allow the application of geometric reconstruction methods which finally give a real model of the vessel (Medina and Wicker 2003; Sanmartín et al. 2006). This geometry is obtained at a specific blood pressure, and consequently unknown initial stresses in equilibrium with this internal load must develop at the artery wall. It is seen, therefore, that an accurate estimation of the initial stresses is needed to correctly describe the material response. A method to account for this stress computation is the inverse analysis in which the effect of the residual strain is neglected (Govindjee et al. 1996; Lu et al. 2007). This assumption is not always valid in arteries (Holzapfel et al. 2007). It should be noted that the numerical simulation and experimental validation of the mechanical response of the human aortic arch under in vivo conditions, including all the aspects mentioned above, is currently a research subject awaiting exploration.

The aim of this work is to analyse the mechanical response of the human aortic arch under in vivo physiological conditions by means of constitutive modelling and numerical simulation. The material and methods considered in this study are presented in Sect. 2. In particular, young and aged arteries without cardiovascular pathologies are considered. The tissue of these two groups is firstly characterised via in vitro tensile test measurements that make it possible to derive via a least-squares procedure the material parameters of a hyperelastic isotropic constitutive model, adopted in this work, to describe the material response. Using these material parameters, Sect. 3 presents the numerical results of the tensile response and, in addition, the simulation of young and aged aortic arches subjected to in vivo conditions with normal and hypertension pressure levels. Relevant aspects related to the geometry, boundary conditions and initial stresses considered in the analysis are specifically detailed. In particular, an alternative methodology to estimate the initial stress field is proposed. The obtained numerical results discussed in Sect. 4 were found to provide a realistic description of the mechanical behaviour of the vessel. Moreover, these predictions, together with an adequate definition of stress/stretch-based criteria, may make it possible to assess the risk of failure at critical zones of the vessel.

2 Materials and methods

2.1 Human aortic arches

The human aortic arches considered in this work have been provided by the Hospital Puerta de Hierro in Madrid. These vessels, obtained according to well-established protocols of the Ethical Committee of the hospital (Goicolea et al. 2006), came from cardiac transplant donors without previous arterial risk factors (i.e. tissues with low cholesterol levels, normal physiological pressure and absence of arterial pathologies of donors with neither smoking nor diabetes records) whose deaths were not related to cardiovascular problems. One of these aortic arches is shown in Fig. 1. This arch configuration is observed in approximately 70% of the population (Al-Okaili and Schwartz 2007).

The present study is focused on two groups selected according to the age of the donors: 16–36 (12 patients) and 65–90 (8 patients). The experimentally measured average diameter and thickness values at different locations of the
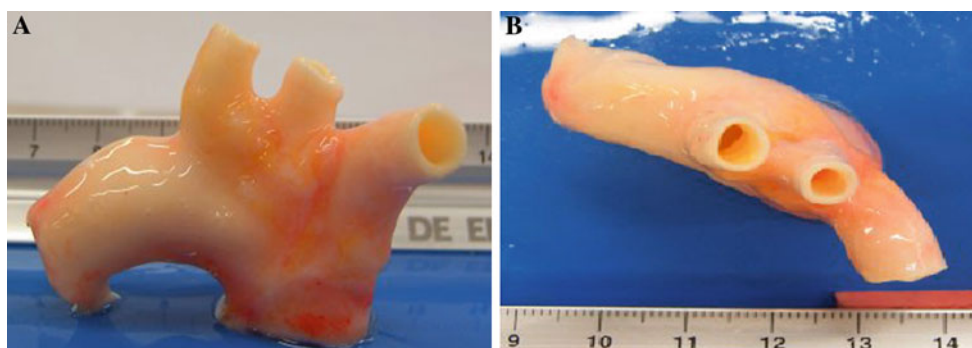

Fig. 1 Human aortic arch: **a** *frontal* view; **b** *top* view

Table 1 Average external diameter and thickness of different parts of aortic arch

	Vessel			
	Brachyo-cephalic trunk	Carotid artery	Subclavian artery	Aorta
Diameter (mm)	12.0 ± 0.34	10.1 ± 0.25	11.2 ± 0.31	24.4 ± 0.45
Thickness (mm)	2.06 ± 0.11	1.89 ± 0.21	2.10 ± 0.08	1.95 ± 0.15

sample are summarised in Table 1. Moreover, the average radius of the arch directrix for both groups was 37 mm ±4.5 (a similar value was reported by Beller et al. (2004)).

2.2 Constitutive modelling

According to the measurements reported in Sect. 3.1, an elastic, isotropic and rate-independent material response is considered for the arteries analysed in the present work. Moreover, their behaviours are taken as incompressible due to the large amount of water present in them (Oijen 2003). To this end, hyperelastic constitutive models can be used to describe their mechanical response (Ogden 1984; Fung 1993; Holzapfel 2000; Doyle et al. 2010, 2012). In this context, a deformation energy function W, assumed to describe the isothermal material behaviour under any loading conditions, is usually defined in terms of the right Cauchy deformation tensor $C = F^{\mathrm{T}} \cdot F$, where F is the deformation gradient tensor and T is the transpose symbol (note that $\det F = 1$ in this case). Invoking classical arguments of continuum mechanics, the Cauchy stress tensor σ is defined as $\sigma = 2F \cdot \frac{\partial W}{\partial C} \cdot F^{\mathrm{T}}$.

In particular, the energy function proposed by Demiray (1972) is expressed as

$$W = \frac{a}{b} \left[\exp \left(\frac{b}{2} (I_1 - 3) \right) - 1 \right], \tag{1}$$

where I_1 is the first invariant of C [$I_1 = \mathrm{tr}(C)$, tr being the trace symbol]. Although this isotropic model is relatively simple (i.e. only depends on I_1), reasonably good responses at high levels of deformation can be predicted with it (Delfino et al. 1997). Only two constants, a and b, are needed for the material characterisation where the parameter a has a clear physical meaning given by the slope at the origin of the Cauchy stress versus the stretch tensile test curve.

As shown in Sect. 3, this constitutive model is adopted in this work to assess its capabilities in the prediction of the mechanical behaviour of a human aortic arch. Although the Demiray model is used in the present study to assess the risk of rupture, it should be noted that it cannot predict the risk of dissection since it does not take into account the layered nature of the tissue.

Moreover, this constitutive model is implemented in an in-house finite-element code extensively validated in many engineering applications where isoparametric elements, including a B-bar technique, are used to avoid numerical locking due to material incompressibility (Celentano 2001).

2.3 Material characterisation via tensile test

In vitro tensile tests were carried out to characterise the mechanical response of the aortic arches considered in the present study. All these tests were performed on the same day using samples obtained immediately after excision (i.e. 1 day from the time of death to testing). The tests were carried out with the specimens permanently submerged in physiological serum (PBS) at a temperature of $37 \pm 0.5°C$. To achieve uniform conditions for each sample, a time interval of 10 min was considered between the end of the assembly and the beginning of the test. To precondition the samples, ten successive loading cycles were executed up to a stress value of 300 kPa. Axial load and axial jaw displacement were recorded during the whole test. Details of the experimental procedure can be found in García-Herrera et al. (2012a).

The uniaxial test measurements reported in Sect. 3.1 are used in this work to determine the material parameters of the Demiray constitutive model briefly presented in Sect. 2.2. For this model, the Cauchy stress associated to the loading direction 1 can be exclusively written in terms of the related axial stretch $\lambda_1 = L/L_0$, with L and L_0 being the current and initial sample lengths, respectively. This relationship reads (Ogden 1984)

$$\sigma_1 = a \left(\lambda_1^2 - \frac{1}{\lambda_1} \right) \exp \left[\frac{b}{2} \left(\lambda_1^2 + \frac{2}{\lambda_1} - 3 \right) \right]. \tag{2}$$

In this case, a linear least-squares-fitting procedure to derive the material parameters a and b is carried out (García-Herrera et al. 2012b). The resulting material parameters for both the young and aged vessels are presented in Sect. 3.1.

3 Results

3.1 Tensile test

The average experimental stress–stretch curves obtained up to the rupture stage along the circumferential direction for both the young and aged groups are plotted in Fig. 2 (the vertical bars denote the standard error, i.e. the ratio between the standard deviation and the square root of the number of specimens), where a good repeatability of the measurements can be clearly observed. Although not shown, the stress–stretch curves along the axial direction exhibited no significant differences with those along the circumferential
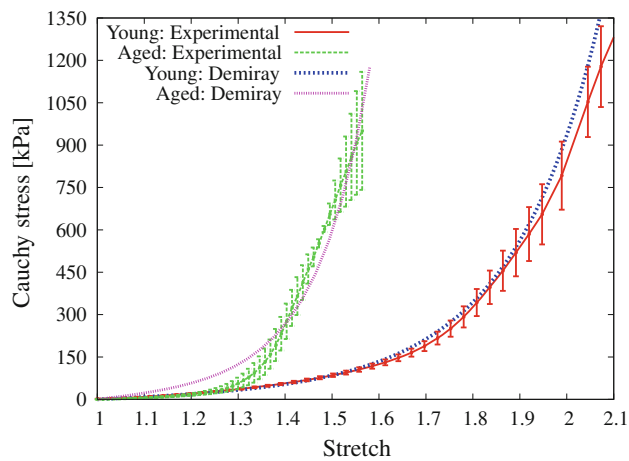
Fig. 2 Experimental measurements and computed results of Cauchy stress versus stretch along circumferential direction for both groups ($r^2_{\text{Young}} = 0.996$ and $r^2_{\text{Aged}} = 0.961$)

Fig. 3 Geometry and boundary conditions of human aortic arch considered in the analysis (dimensions in millimeters)

Table 2 Groups considered in study: age interval and material parameters

Group	Age	Material parameters	
		a (kPa)	b
Young	16–36	104.0	0.844
Aged	65–90	69.2	5.792

3.2 Simulation of an aortic arch

This section presents the numerical simulation of the mechanical response of young and aged human aortic arches under in vivo normal and hypertension physiological conditions, i.e. systolic pressure of 120 and 160 mmHg, respectively. To this end, important aspects related to this analysis are presented separately in what follows.

3.2.1 Geometry and boundary conditions

The geometry of the human aortic arch used in the numerical simulation carried out in this work was obtained from anatomical data of adults (Putz et al. 2001; Beller et al. 2005) and from the samples considered in Sect. 2.1. The geometric configuration corresponds to the arch subjected to diastolic pressure (80 mmHg). It should be noted that the initial stresses resulting from this condition must be taken into account in the simulation; otherwise, the response is fictitiously flexible. This aspect is described in Sect. 3.2.2. Figure 3 depicts the geometry of the human aortic arch considered in the present analysis.

In vivo measurements on healthy patients during their cardiac cycle reported by Beller et al. (2004) are adopted here to define appropriate boundary conditions. They encompass three types of kinematic constraints. Firstly, the axial motion of the aortic root, caused by its connection to the left ventricle, consisting in an axial displacement of $u = 8.9$ mm and a rotation of $\phi_0 = 6°$; see Figs. 3 and 4. Secondly, the other four edges of the aortic arch are assumed to be axially fixed and unconstrained along the radial direction. Thirdly, the effect of the ligamentum arteriosum is taken into account by means of a spring element with a stiffness ten times higher than that of the aortic arch tissue. The influence of this ligamentum on

direction in a wide stretch range ([1.0–2.1] and [1.0–1.6] for the young and aged samples, respectively). Thus, the behaviour can be assumed to be practically isotropic since its stiffness is mainly provided by the elastin component of the tissue. Moreover, it should be noted that similar material responses were observed at different positions around the circumference and along the length of the artery. Therefore, these two aspects (i.e. material isotropy and homogeneity) justify the assumption that an adequate description of the material behaviour can be simply tackled by means of the constitutive model expressed by Eq. 1. In addition, the tensile response of arteries belonging to healthy patients between 37 and 51 years old (not shown here) exhibits an intermediate response between those presented in Fig. 2.

The stress–stretch curves obtained by applying a least-squares fitting of Eq. 2 to the corresponding experimental data are also plotted in Fig. 2. The material parameters derived with this methodology are included in Table 2. A detailed description of this material characterisation procedure is reported in García-Herrera et al. (2012b). These parameters are used in the simulations presented in Sect. 3.2.3.
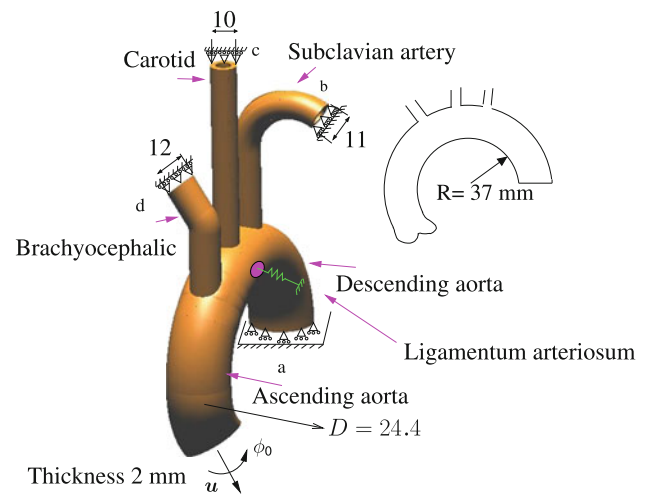
Fig. 4 Motion of aortic root (Beller et al. 2004)
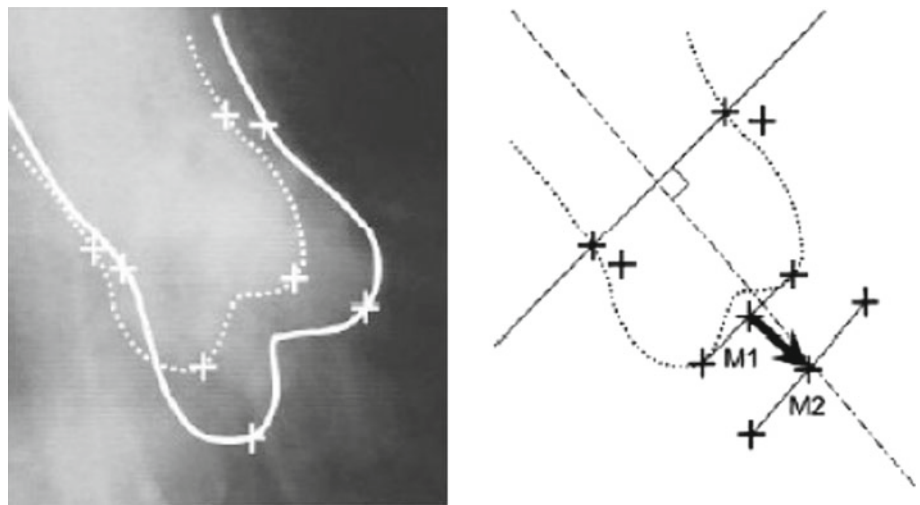
Table 3 First estimation for initial stress components of arteries at a pressure of 80 mmHg

Vessel	σ_θ (kPa)	σ_z (kPa)
Aortic arch	65.1	32.6
Brachyocephalic trunk	32.0	16.0
Carotid artery	26.7	13.4
Subclavian artery	26.7	13.4

the mechanical response of the aortic arch under extreme scenarios was described by Richens et al. (2002) and Richens et al. (2004). All these boundary conditions are shown in Fig. 3.

3.2.2 Estimation of initial stresses

The in vivo initial stresses present in the different arteries of the aortic arch are estimated in this work for the diastolic pressure (80 mmHg), together with and axial stretch of 1.2 according to the measurements reported by Chuong and Fung (1986). Both the circumferential σ_θ and axial σ_z components of the stress tensor are firstly computed with the thin-walled equation for cylinders (García-Herrera et al. 2012a). The assumption of constant stress along the wall thickness is justified by the long-recognised fact that the main purpose of the initial hoop stress radial distribution that develops along an artery wall is the achievement of a nearly uniform stress pattern in the vessel when it is subjected to standard physiological loading states (Fung 1993; Okamoto et al. 2002). The obtained values for the initial circumferential and axial stress components are summarised in Table 3. However, this computed initial stress field does not strictly fulfil, in general, the equilibrium with the internal pressure (80 mmHg). This drawback is overcome via the numerical procedure described in what follows.
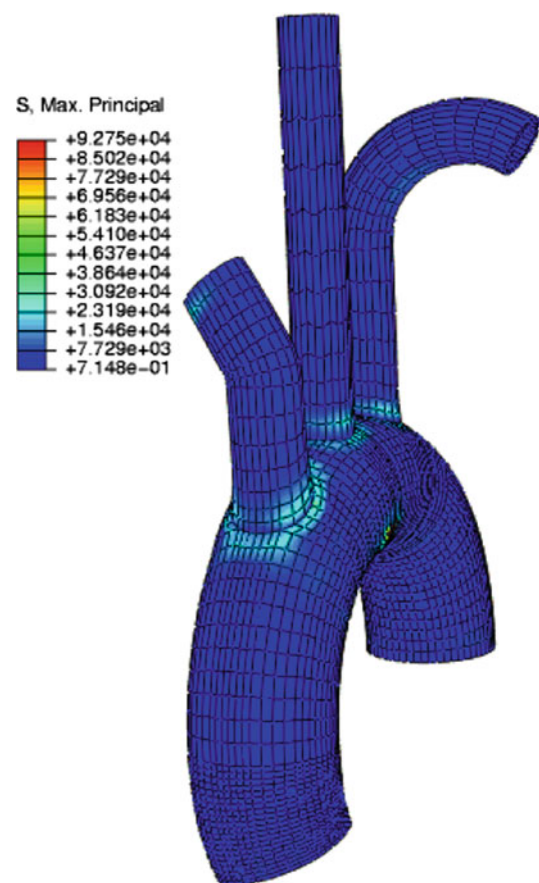

Fig. 5 Computed initial maximum principal stress at 80 mmHg

The approach to obtaining a compatible initial stress field is iteratively tackled by solving the equilibrium equations together with the Demiray constitutive model using the finite-element method (García-Herrera et al. 2012b) until the condition of a nearly zero displacement field for the whole aortic arch is fulfilled. For this problem, a maximum admissible diameter variation of 2% was chosen. The converged
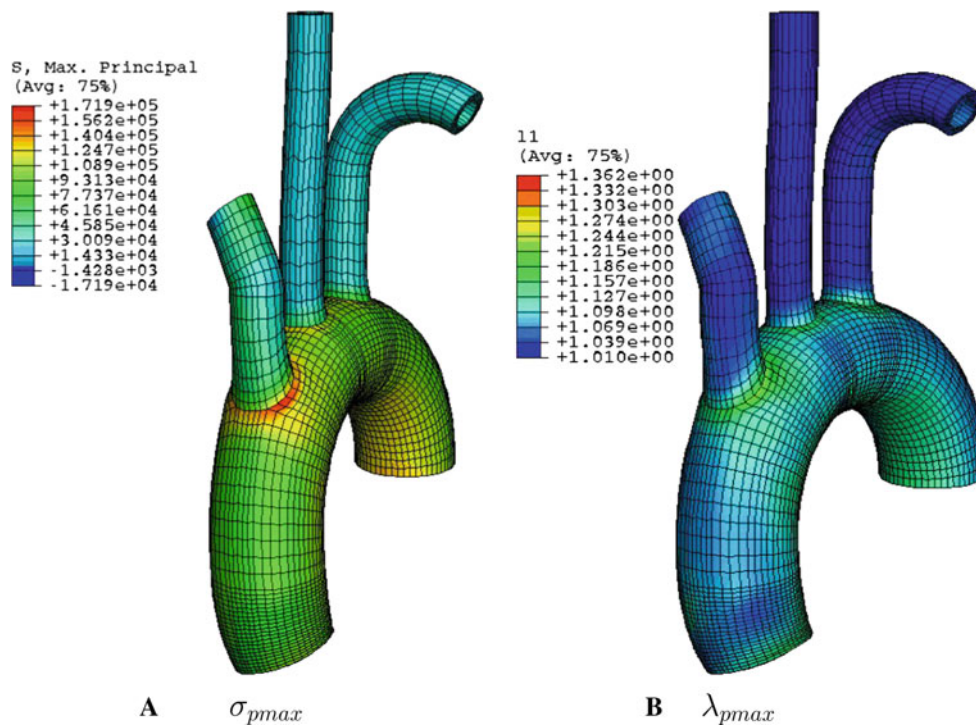
Fig. 6 Deformed configuration for young aortic arch at 120 mmHg. **a** Maximum principal stress (Pa). **b** Maximum principal stretch

initial maximum principal stress field obtained with this procedure, which is considered in the simulations presented in Sect. 3.2.3, is shown in Fig. 5. It is seen that the stresses are mainly concentrated in the vicinity of the bifurcations and ligamentum arteriosum. Although the stress distribution is not uniform along the thickness, the corresponding average values nearly agree with those summarised in Table 3. It should be noted that the stress concentrations located around these zones were found to be not strongly affected by the curvature radii of the junctions of the branches from the aorta.

3.2.3 Stress and stretch contours

As mentioned previously, the mechanical response of a human aortic arch is simulated under in vivo normal and hypertension physiological conditions. In the first case, a systolic pressure of 120 mmHg is applied to the young aortic arch. In the second case, the effect of hypertension pressure of 160 mmHg on young and aged vessels is analysed.

The simulations were carried out using the non-linear constitutive model and the corresponding material parameters respectively presented in Sects. 2.2 and 3.1.

The finite-element mesh used in the simulations was composed of 28,437 nodes and 22,176 isoparametric hexahedra. Four elements were considered along the wall thickness in order to properly capture the stress radial gradients that may

develop in the different regions of the aortic arch. It should be noted that this mesh is the result of a previous convergence study of the numerical response to different discretisations.

The maximum principal stress and stretch contours at the deformed configuration for a young aortic arch subjected to 120 mmHg are plotted in Fig. 6. The same results at 160 mmHg for young and aged aortic arches are respectively shown in Figs. 7 and 8. In addition, the radial, circumferential and longitudinal stress components computed for the hypertension conditions for both groups are respectively depicted in Figs. 9 and 10.

4 Discussion

The experimental tensile curves shown in Fig. 2 exhibit two zones with different stiffnesses. For low stretching, the curves show a flexible response with a nearly constant slope. This first zone ranges up to $\lambda_1 \simeq 1.35$ and $\lambda_1 \simeq 1.20$ for the young and aged samples, respectively. For larger stretches, the slope continuously increases up to the rupture stage. Although some experimental-numerical discrepancies are noticed (e.g. at high and low levels of deformation for the young and aged samples, respectively), an overall good adjustment is clearly seen within the full stretching range for both groups. Moreover, additional experimental tensile tests (not shown) using samples extracted from regions located near the arterial bifurcations showed a similar response to that corresponding to

Fig. 7 Deformed configuration for young aortic arch at 160 mmHg. **a** Maximum principal stress (Pa). **b** Maximum principal stretch

A σ_{pmax} B λ_{pmax}

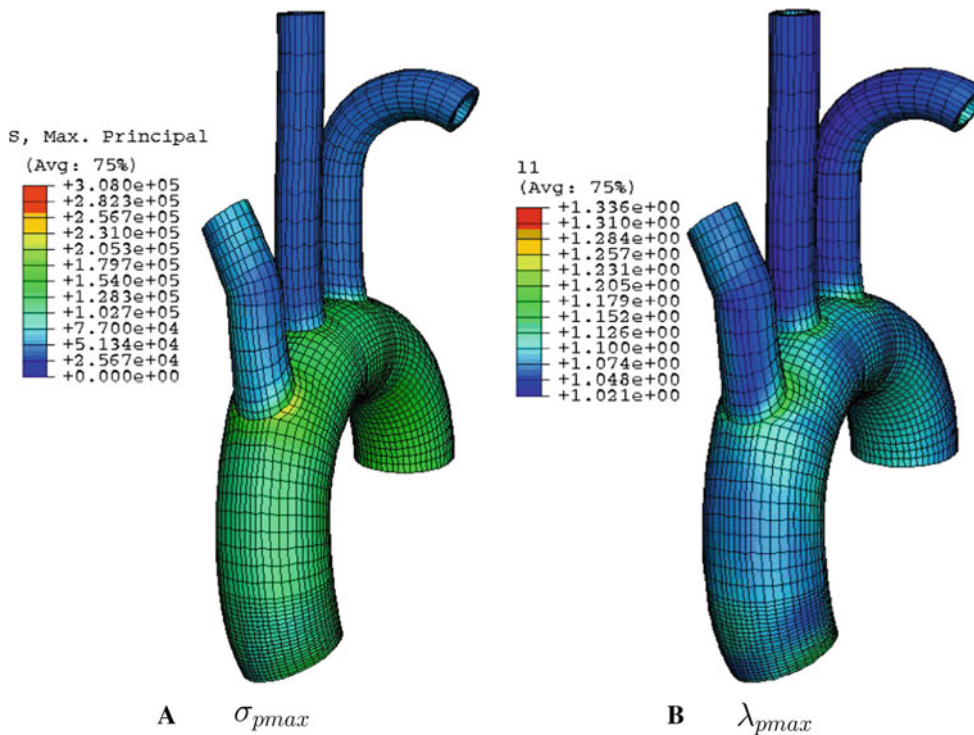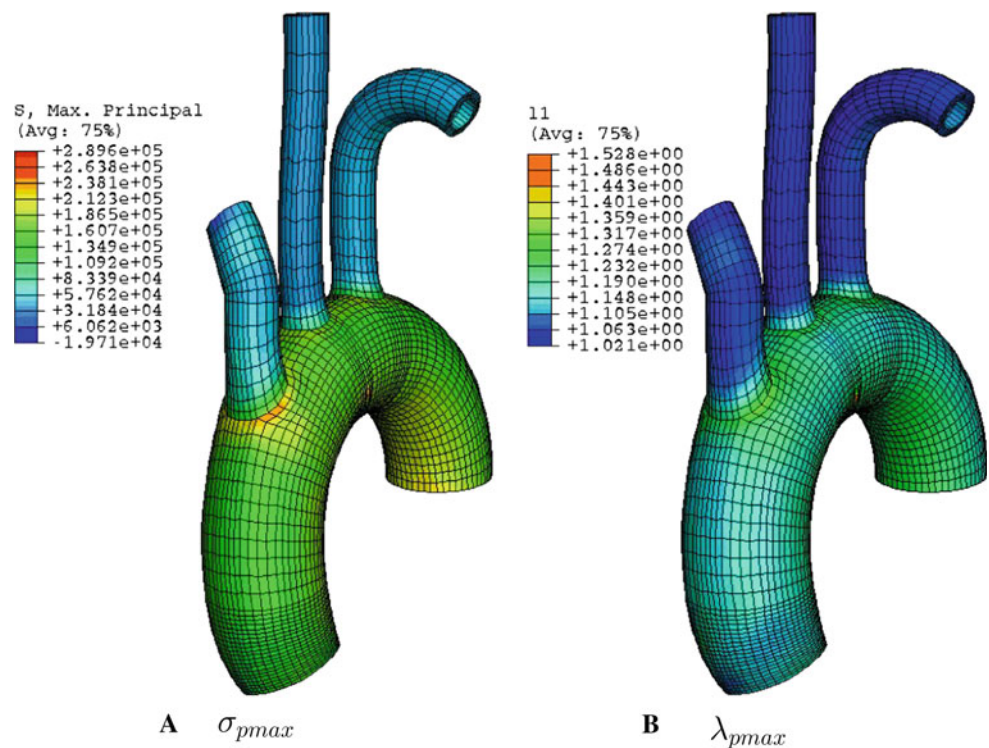A σ_{pmax} B λ_{pmax}

Fig. 8 Deformed configuration for aged aortic arch at 160 mmHg. **a** Maximum principal stress (Pa). **b** Maximum principal stretch

the aortic arch (e.g. within the stretch range [1.0–1.6], the responses are practically the same, while a difference of 40% is observed for a stretch value of 2.0). The discrepancy at high stretch levels can be attributed to the action of the complexly oriented collagen fibres. This effect has also been reported by Hariton et al. (2007). The assumption of homogeneous
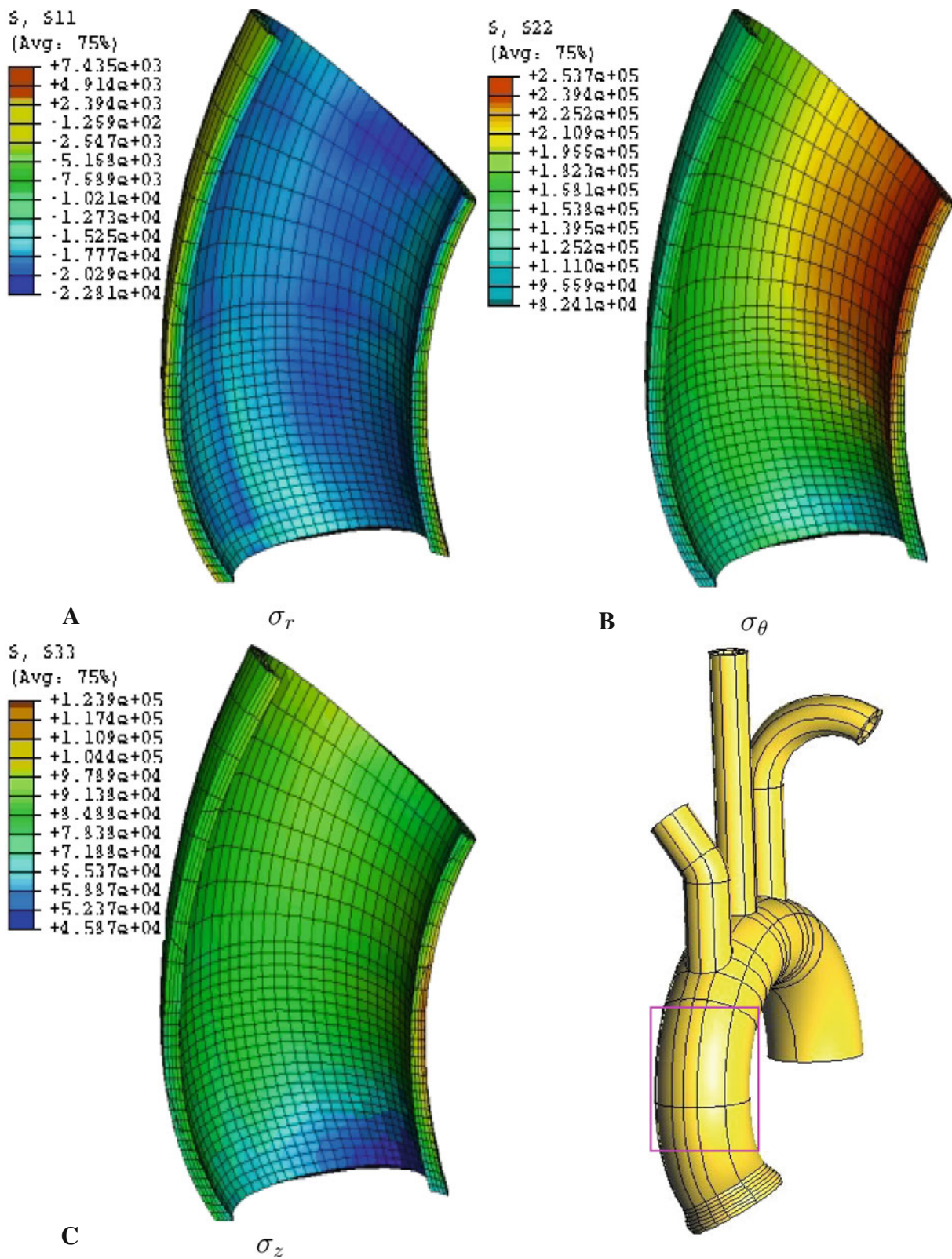
Fig. 9 Deformed configuration for young aortic arch at 160 mmHg: **a** radial, **b** circumferential and **c** longitudinal stress components (Pa)

mechanical properties along the whole arch is clearly a limitation of the present analysis.

The use of the maximum principal stress and stretch values that develop in loaded aortas has been proposed in the
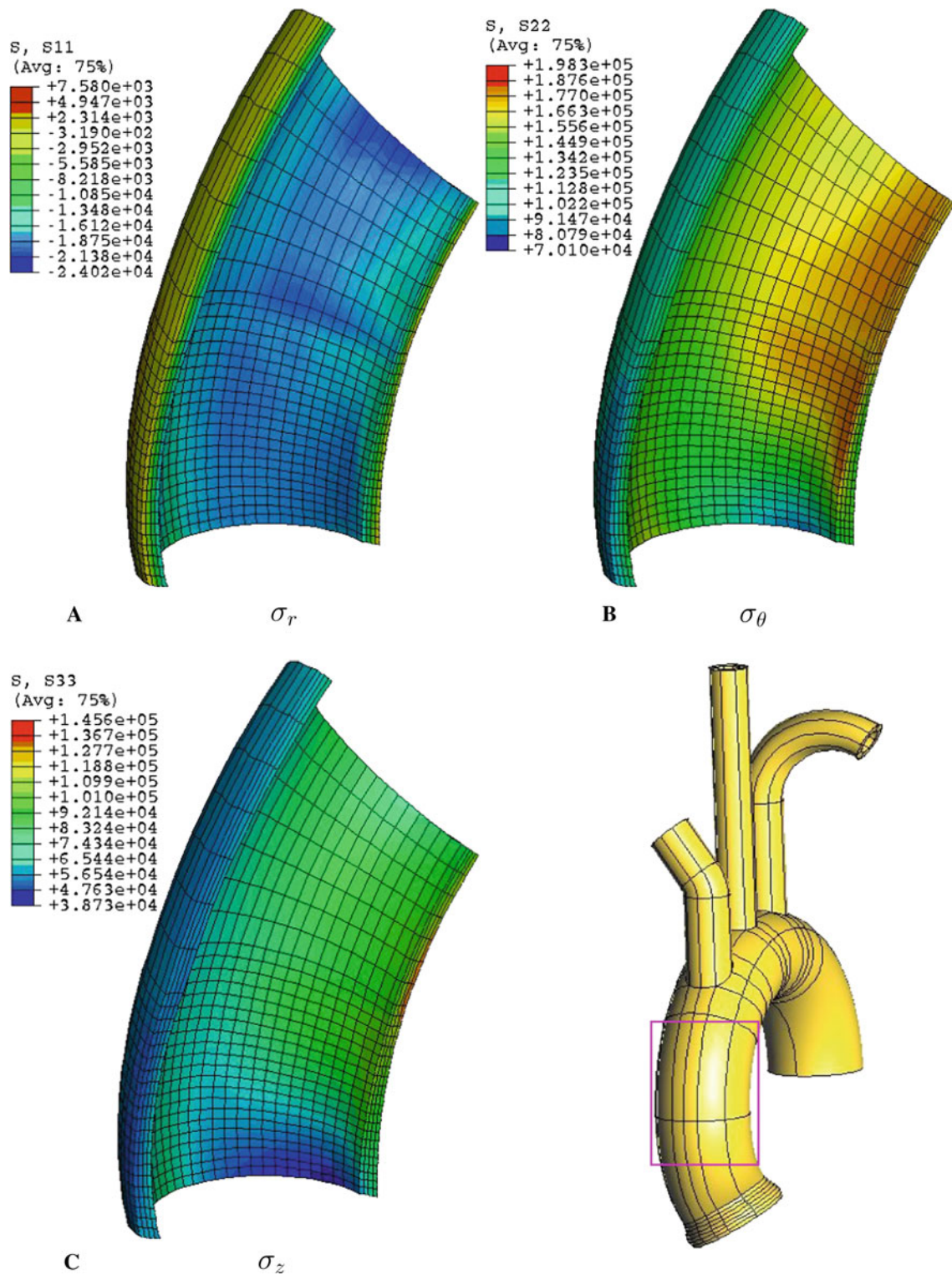
Fig. 10 Deformed configuration for aged aortic arch at 160 mmHg: **a** radial, **b** circumferential and **c** longitudinal stress components (Pa)

literature to predict the failure of a vessel. In particular, this problem has been studied by Di Martino and Vorp (2003); Li and Kleinstreuer (2005) and Vorp (2007) defining a maximum principal-stress-based criterion for descending aortas

with aneurysms. Moreover, other authors, such as Mohan and Melvin (1982) and Lonescu et al. (2006), proposed failure criteria for soft tissues in terms of maximum stretches. In these approaches, the maximum principal stress and stretch

values are compared to those measured in the tensile test. In the present work, these two variables are also adopted to assess the failure degree of the aortic arch under normal and hypertension loading conditions.

As depicted in Fig. 6a, the maximum stress values for the young group at the normal physiological condition occur at the intersection of the brachyocephalic trunk with the arch. For the ascending aorta, the maximum stress value is 143 kPa, well below the tensile rupture stress for the young group (i.e. 1,270 kPa; Fig. 2). Moreover, relevant stress levels are developed at the internal region of the arch. As depicted in Fig. 6b, the maximum stretch value of 1.36 is located at the inner wall of the brachyocephalic trunk—arch union. This value corresponds to 65% of the rupture stretch (i.e. 2.1; Fig. 2). Both failure criteria clearly show that the zones with higher risk levels are situated at the root of the three aortic arch bifurcations and at the vicinity of the ligamentum arteriosum. From a clinical point of view, the most important zone is that located near the ligamentum arteriosum due to the high stress concentration that takes place there (Pasic et al. 2000; Chiesa et al. 2003; Richens et al. 2004; Field et al. 2007; McGillicuddy and Rosen 2007; Braverman et al. 2010). The stress level in this area is more critical than those developed at the junctions where arteries branch off from the aortic arch. However, relevant stresses can occur in all these regions under extreme loading conditions (e.g. hypertension, automobile accidents).

Although the systolic pressure P_s does not significantly affect the stress level compared to the diastolic pressure P_d (Figs. 6a and 5), relatively large strains are developed in the ascending aorta due to the kinematic boundary conditions. The external diameter and average thickness of the ascending aorta at 120 mmHg are 26.1 and 1.61 mm, respectively. The external diameters of the ascending aorta at the diastolic and systolic conditions (D_d and D_s, respectively) allow the estimation of its stretching capacity. This feature is usually quantified by means of the distensibility DC (Laurent et al. 2006):

$$DC = \frac{D_s^2 - D_d^2}{D_s^2(P_s - P_d)}, \tag{3}$$

where, in this case, the distensibility gives 2.7×10^{-3} mmHg^{-1}, which is very close to the in vivo measured value of 2.5×10^{-3} mmHg^{-1} in healthy young patients (Koullias et al. 2005).

Figure 7 shows that the maximum stress and stretch values for the young group at the hypertension condition (290 kPa and 1.6 respectively) are, as in the former case, also mainly located near the root of the three aortic arch bifurcations and in the vicinity of the ligamentum arteriosum. Considering these values in the stress–stretch curve of Fig. 2, it is seen that the material behaves within the so-called elbow zone (defined approximately by the interval $1.55 < \lambda_1 < 1.85$),

which exhibits a moderate stiffness that allows the damping of the pressure wave with stretch levels smaller than that of the rupture stage (the ratio between these two values is 0.73).

The maximum stress and stretch values for the aged aortic arch at the hypertension condition are, as plotted in Fig. 8, 300 kPa and 1.33 respectively. The aged aortic arch exhibits, compared to that of the young group, a stiffer material response with lower stretching levels. This stress–stretch level is beyond the elbow zone of this material (defined approximately in this case by the interval $1.25 < \lambda_1 < 1.40$), which consequently leads to a deterioration of the pressure wave damping capacity of the artery reflected in the development of more irregular downstream flows and pressures. It should be noted that the maximum stresses under in vivo conditions occur for stretch values higher than 1.4, where the tensile fitting is adequate (Fig. 2). This fact is also appreciated in the drop of the distensibility to a value of 1.3×10^{-3} mmHg^{-1}, which is very close to the in vivo measured values of aged arteries (Liu et al. 2012) and nearly 50% less than that of a healthy young patient. This marked decrease in distensibility with age has been also reported by Rose et al. (2010). Moreover, the ratio between the maximum stretch value and that of the tensile rupture stage (Fig. 2) is 0.85 in this case, i.e. closer to the failure condition than that of the young aortic arches.

The stress distributions in the ascending aorta at 160 mmHg are depicted in detail in Figs. 9 and 10 for the young and aged patients respectively. For the young tissue, the maximum stress occurs at the inner part of the aortic arch, e.g. the respective values for the circumferential and longitudinal stress components are 250 and 125 kPa. It should be noted that the value of the radial stress component at the internal surface of the aorta evens up the applied pressure (i.e. 160 mmHg= 21.332 kPa). A similar stress pattern is also observed for the aged tissue, where in this case the maximum circumferential and longitudinal stress components are 200 and 146 kPa respectively. Moreover, different circumferential stress values at the inner and outer parts of the aortic arch are clearly observed for both tissues.

Finally, it should be mentioned that additional simulations carried out with different boundary conditions and lengths of the three arteries (i.e. brachyocephalic trunk, carotid artery and subclavian artery) showed that they do not substantially affect the stress contours at the root of those arteries.

5 Conclusions

Constitutive modelling and numerical simulation aimed at analysing the mechanical response of young and aged human aortic arches under in vivo physiological conditions was presented. The tissue of these two groups were firstly characterised via in vitro tensile test measurements that enabled,

via a least-squares procedure, the derivation of the material parameters of a hyperelastic isotropic constitutive model adopted in this work to describe the material response. This material characterisation, together with the proposed alternative methodology to estimate the initial stress, was found to provide a realistic description of the mechanical behaviour of the aortic arch subjected to in vivo normal and hypertension pressures. The maximum principal stress and stretch values adopted here as risk-of-failure criteria allowed the determination of the critical zones of the vessel. These two failure criteria clearly showed that the zones with higher risk levels are situated at the root of the three aortic arch bifurcations and in the vicinity of the ligamentum arteriosum for both groups of patients. For the healthy young patients, the computed distensibility was very similar to an experimentally measured value reported in the literature. In addition, the predicted distensibility for the aged tissue was very close to the measured value of pathological arteries, which approximately corresponds to 50% lower than that of the young vessel.

Future research on this area will be focused on the limitations of the present analysis, i.e. consideration of patient-specific complex geometry and realistic boundary conditions aimed at achieving a better estimation of the stress and strain patterns in the artery, further validation including more results than those considered in this work, assessment of other constitutive models, effects of the presence of aneurysms, characterisation of the mechanical response of the ligamentum arteriosum in order to more accurately compute the stress concentrations and, in addition, simulation of the influence of blood flow on the mechanical response of the aortic arch.

Conflict of interest The authors have no conflicting interests associated with this paper.

References

Al-Okaili R, Schwartz ED (2007) Bilateral aortic origins of the vertebral arteries with right vertebral artery arising distal to left subclavian artery: case report. Surg Neurol 67:174–176

Beller CJ, Labrosse MR, Thubrikar MJ, Robicsek F (2004) Role of aortic root motion in the pathogenesis of aortic dissection. Circulation 109:763–769

Beller CJ, Labrosse MR, Thubrikar MJ, Szabo G, Robicsek F, Hagl S (2005) Increased aortic wall stress in aortic insufficiency: clinical data and computer model. Eur J Cardiothorac Surg 27:270–275

Braverman A, Thomson R, Sanchez L (2010) Braunwald's heart disease (Chapter 60: Diseases of the aorta), 9th edn. Elsevier, Philadelphia

Celentano D (2001) A large strain thermoviscoplastic formulation for the solidification of S.G. cast iron in a green sand mould. Int J Plast 17:1623–1658

Chiesa R, Moura M, Lucci C, Castellano R, Civilini E, Melissano G, Tshomba Y (2003) Blunt trauma to the thoracic aorta: mechanisms involved, diagnosis and management. J Vasc Bras 2(3):197–209

Chuong CJ, Fung YC (1986) On residual stresses in arteries. ASME J Biomech Eng 108:189–192

De Caro E, Trocchio G, Smeraldi A, Calevo MG, Pongiglione G (2007) Aortic arch geometry and exercise-induced hypertension in aortic coarctation. Am J Cardiol 99:1284–1287

Delfino A, Stergiopulos N, Moore J, Meister J (1997) Residual strain effects on the stress field in a thick wall finite element model of the human carotid bifurcation. J Biomech 30:777–786

Demiray H (1972) On the elasticity of soft biological tissues. J Biomech 5:309–311

Di Martino ES, Vorp DA (2003) Effect of variation in intraluminal thrombus constitutive properties on abdominal aortic aneurysm wall stress. Ann Biomed Eng 31:804–809

Doyle BJ, Cloonan AJ, Walsh MT, Vorp DA, McGloughlin TM (2010) Identification of rupture locations in patient-specific abdominal aortic aneurysms using experimental and computational techniques. J Biomech 43:1408–1406

Doyle BJ, Killion J, Callanan A (2012) Use of the photoelastic method and finite element analysis in the assessment of wall strain in abdominal aortic aneurysm models. J Biomech 45:1759–1768

Erbel R, Eggebrecht H (2006) Aortic dimensions and the risk of dissection. Heart 92:137–142

Ergin MA, Spielvogel D, Apaydin A, Lansman SL, McCullough JN, Galla JD, Griepp RD (1999) Surgical treatment of the dilated ascending aorta: when and how? Ann Thorac Surg 67:1834–1839

Field M, Richens D (2006) Anticipatory valsalva-type response as a contributory factor in low impact blunt traumatic aortic rupture. Med Hypotheses 67:87–92

Field M, Sastry P, Zhao A, Richens D (2007) Small vessel avulsion and acute aortic syndrome: a putative aetiology for initiation and propagation of blunt traumatic aortic injury at the isthmus. Med Hypotheses 68:1392–1398

Fung Y (1993) Biomechanics. Mechanical properties of living tissues. Springer, New York

Gao F, Watanabe M, Matsuzawa T (2006) Stress analysis in a layered aortic arch model under pulsatile blood flow. Biomed Eng Online 5:25

García-Herrera CM, Celentano DJ, Cruchaga MA, Rojo FJ, Atienza JM, Guinea GV, Goicolea JM (2012a) Mechanical characterisation of the human thoracic descending aorta: experiments and modelling. Comput Methods Biomech Biomed Eng 15:185–193

García-Herrera CM, Celentano DJ, Cruchaga MA (2012b) Bending and pressurisation test of the human aoritc arch: experiments, modelling and simulation of a patient-specific case. Comput Methods Biomech Biomed Eng (in press)

Goicolea J, Atienza JM, Burgos R, García-Touchard A, Goicolea J, Guinea G, Mingo S, Montero C, Salas C (2006) Biomecánica aórtica y su correlación in vivo, estudio del comportamiento mecánico y de la rotura de aorta y su correlación ecocardiográfica, histológica y molecular. Protocolo de extracción de muestras. Hospital Universitario Puerta de Hierro, Madrid

Govindjee S, Mihalic PA (1996) Computational methods for inverse finite elastostatics. Comput Methods Appl Mech Eng 136:47–57

Holzapfel GA (2000) Non linear solid mechanics. Wiley, West Sussex

Hariton I, deBotton G, Gasser TC, Holzapfel GA (2007) Stress-modulated collagen fiber remodeling in a human carotid bifurcation. J Theor Biol 248:460–470

Holzapfel GA, Sommer G, Auer M, Regitnig P, Ogden RW (2007) Layer-specific 3D residual deformations of human aortas with non-atherosclerotic intimal thickening. Ann Biomed Eng 35:530–545

Koullias G, Modak R, Tranquilli M (2005) Mechanical deterioration underlies malignant behavior of aneurysmal human ascending aorta. J Thorac Cardiovasc Surg 130:677.e1–677.e9

Laurent S, Cockcroft J, Bortel LV, Boutouyrie P, Giannattasio C, Hayoz D, Pannier B, Vlachopoulos C, Wilkinson I, Struijker-Boudier H (2006) Expert consensus document on arterial stiffness: methodological issued and clinical applications. Eur Heart J 27:2588–2605

Li Z, Kleinstreuer C (2005) A new wall stress equation for aneurysm-rupture prediction. Ann Biomed Eng 33:209–213

Liu CY, Chen D, Teixido-Tura G, Chugh AR, Redheuil A, Gomes AS, Prince MR, Hundley W, Bluemke DA, Lima JA (2012) Aortic size, distensibility, and pulse wave velocity changes with aging: longitudinal analysis from Multi-Ethnic Study of Atherosclerosis (MESA). J Cardiovasc Magn Reson 14:126–127

Lonescu I, Guilkey JE, Berzins M, Kirby RM, Weiss JA (2006) Simulation of soft tissue failure using the material point method. J Biomech Eng 128:917–924

Lu J, Zhou X, Raghavan ML (2007) Inverse elastostatic stress analysis in pre-deformed biological structures: demostration using abdominal aortic aneurysms. J Biomech 40:693–696

McGillicuddy D, Rosen P (2007) Diagnostic dilemmas and current controversies in blunt chest trauma. Emerg Med Clin N Am 25:695–711

Medina F, Wicker RB (2003) Geometric modeling of the human aorta for rapid prototyping using patient data and commercial software packages. Summer bioengineering conference, Florida, USA

Mohan D, Melvin J (1982) Failure properties of passive human aortic tissue. I uniaxial tension test. J Biomech 15(11):887–902

Nichols W, Rourke MO (1990) McDonald's flow in arteries theoretical, experimental and clinical principles, 3rd edn. Oxford University, New York

Ogden RW (1984) Non-linear elastic deformations. Dover, New York

Oijen CV (2003) Mechanics and design of fiber-reinforced vascular prostheses. Ph.D. thesis, Technische Universiteit Eindhoiven

Okamoto RJ, Wagenseil JE, DeLong WR, Peterson SJ, Kouchoukos NT, Sundt TM III (2002) Mechanical properties of dilated human ascending aorta. Ann Biomed Eng 30:624–635

Pape LA, Tsai TT, Isselbacher EM, Oh JK, O'Gara PT, Evangelista A, Fattori R, Meinhardt G, Trimarchi S, Bossone E, Suzuki T, Cooper JV, Froehlich JB, Nienaber CA, Eagle KA (2007) Aortic diameter ≥5.5 cm is not a good predictor of type A aortic dissection. Observations from the international registry of acute aortic dissection (IRAD). Circulation 116:1120–1127

Pasic M, Ewert R, Engel M, Franz N, Bergs P, Kuppe H, Hetzer R (2000) Aortic rupture and concomitant transection of the left bronchus after blunt chest trauma. Chest 117:1508–1510

Putz R, Pabst R, Weiglein A (2001) Sobotta atlas of human anatomic atlas, vol 2. Lippincott Williams & Wilkins, Philadelphia

Richens D, Field M, Neale M, Oakley C (2002) The mechanism of injury in blunt traumatic rupture of the aorta. Eur J Cardiothorac Surg 21:288–293

Richens D, Field M, Hashim S, Neale M, Oakley C (2004) A finite element model of blunt traumatic aortic rupture. Eur J Cardiothorac Surg 25:1039–1047

Rose JL, Lalande A, Bouchot O, Bourennane EB, Walker PM, Ugolini P, Revol-Muller C, Cartier R, Brunotte F (2010) Influence of age and sex on aortic distensibility assessed by MRI in healthy subjects. Magn Reson Imaging 28:255–263

Sanmartín M, Goicolea J, García C, García J, Crespo A, Rodríguez J, Goicolea JM (2006) Influencia de la tensión de cizallamiento en la reestenosis intra-stent: Estudio in vivo con reconstrucción 3D y dinámica de fluidos computacional. Rev Española Cardiol 59(1): 20–27

Vorp DA (2007) Biomechanics of abdominal aortic aneurysm. J Biomech 40:1887–1902